ResearchGate

See discussions, stats, and author profiles for this publication at: https://www.researchgate.net/publication/10974636

Substitution of Conserved Hydrophobic Residues in Motifs B and C of HIV-1 RT Alters the Geometry of Its Catalytic Pocket †

ARTICLE *in* BIOCHEMISTRY · JANUARY 2003

Impact Factor: 3.02 · DOI: 10.1021/bi026311z · Source: PubMed

CITATIONS
14

READS
25

5 AUTHORS, INCLUDING:

Bechan Sharma
University of Allahabad
111 PUBLICATIONS **1,278** CITATIONS
SEE PROFILE

Kamalendra Singh
Rutgers New Jersey Medical School
59 PUBLICATIONS **858** CITATIONS
SEE PROFILE

Virendra Pandey
Rutgers New Jersey Medical School
87 PUBLICATIONS **1,741** CITATIONS
SEE PROFILE

Available from: Virendra Pandey
Retrieved on: 31 January 2016

Substitution of Conserved Hydrophobic Residues in Motifs B and C of HIV-1 RT Alters the Geometry of Its Catalytic Pocket†

Bechan Sharma, Neerja Kaushik,* Kamalendra Singh, Suriender Kumar, and Virendra N. Pandey*

Department of Biochemistry and Molecular Biology, Center for the Study of Emerging and Re-Emerging Pathogens, University of Medicine and Dentistry of New Jersey, New Jersey Medical School, 185 South Orange Avenue, Newark, New Jersey 07103

Received June 18, 2002; Revised Manuscript Received October 8, 2002

ABSTRACT: Recent crystallographic data suggest that a number of hydrophobic residues seen clustered between the structurally conserved $\alpha\beta\beta\alpha$ motif of the palm subdomain and at the junction of palm and fingers subdomains of human immunodeficiency virus type 1 reverse transcriptase (HIV-1 RT) provide an optimal geometry to the $\alpha\beta$ sandwich of the palm subdomain, which harbors the catalytic site and the primer-binding grip region. This region has also been implicated in binding to the non-nucleoside RT inhibitors. We have evaluated the impact of conserved and nonconserved amino acid substitutions at four hydrophobic positions in this region of HIV-1 RT, in the context of their biochemical characteristics. The residues that have been analyzed include Ile-167, Leu-187, and Val-189 which are located within the $\alpha\beta\beta\alpha$ motif, while Trp-153 lies next to the conserved LPQG motif, at the juncture of the palm and fingers subdomains. Our results show that all substitutions at I167 with the exception of I167T were deleterious to enzyme function in contrast to substitutions at V189 which enhanced the enzymatic activity. Ala substitution at residues W153 and L187 also substantially hindered the polymerase function of the enzyme. Further analysis revealed that the defective mutant derivatives of I167 were substantially impaired in their apparent dNTP binding abilities, thereby impacting the geometry of the dNTP binding pocket. The extent of misinsertion and misincorporation was higher in the case of RT variants of W153 and V189, specifically on a DNA template. Interestingly, none of the mutant derivatives of these residues were resistant to nucleoside inhibitors. A salient finding was that all nonconserved mutants of these residues exhibited hypersensitivity to nevirapine. We have analyzed these findings and their significance in the context of the HIV-1 RT structure and propose that these residues exert their effect via their indirect interactions with the template-primer through residues in their vicinity.

The human immunodeficiency virus type 1 reverse transcriptase (HIV-1 RT)[1] is essential for the conversion of viral genomic RNA into a double-stranded DNA intermediate, which is integrated into the host cell genome (*1*−*3*). RT is a multifunctional enzyme that possesses RNA- and DNA-dependent DNA polymerase and RNase H activities (*3*). In the HIV-1 virion, its RT exists as a heterodimer (*4*), consisting of two polypeptides, i.e., p66 and its protease cleavage product p51 (*4*−*6*). The polymerase domain of p66 assumes an open conformation and folds into four distinct subdomains designated as fingers, palm, thumb, and connection subdomains (*7*). The polymerase domain of the p51 subunit is closed and acquires a different arrangement of these subdomains. This asymmetric dimeric form of HIV-1 RT is thermodynamically favorable and biologically viable in contrast to the monomeric forms of the individual subunits, which exhibit little or no catalytic activity (*8*). In vitro, HIV-1 RT also exists as a homodimer, exhibiting biochemical and kinetic characteristics similar to those of the heterodimeric enzyme (*9*). Although the p51 subunit has also been suggested to exist as a homodimer, we have recently demonstrated that it mainly exists in a monomeric form (*10*).

The availability of high-resolution X-ray crystal structures of HIV-1 RT in unliganded form (*11*, *12*) and liganded with non-nucleoside inhibitors (*7*, *13*−*16*), RNA−DNA hybrid (*17*), double-stranded DNA (*18*, *19*), and with DNA−dNTP (*20*) has greatly facilitated the analysis and understanding of the various mechanistic aspects of this enzyme. These structural studies in conjunction with biochemical evaluation of recombinant HIV-1 RT variants have led to the identification of mutations impacting substrate dNTP binding and/or selection, drug resistance, and fidelity parameters. For instance, the interaction of DNA polymerases

† This research was supported by a grant from the National Cancer Institute, National Institutes of Health (CA72821).

* To whom correspondence should be addressed. Telephone: (973) 972-0660 and (973) 972-8653. Fax: (973) 972-8657 and (973) 972-5594. E-mail: pandey@umdnj.edu and kaushik@umdnj.edu.

[1] Abbreviations: SDS−PAGE, sodium dodecyl sulfate−polyacrylamide gel electrophoresis; DTT, dithiothreitol; PMSF, phenylmethanesulfonyl fluoride; IPTG, isopropyl β-thiogalactopyranoside; poly(rA)·$(dT)_{18}$, polyriboadenylic acid annealed with $(oligodeoxythymidylic\ acid)_{18}$; dNTP, deoxyribonucleoside triphosphate; dATP, dCTP, dGTP, and dTTP, nucleoside triphosphates of deoxyadenosine, deoxycytidine, deoxyguanosine, and thymidine, respectively; HIV-1 RT, human immunodeficiency virus type 1 reverse transcriptase; IMAC, immobilized metal affinity chromatography; U5-PBS HIV-1 RNA template, HIV-1 genomic RNA template corresponding to the primer binding sequence region; U5-PBS HIV-1 DNA template, DNA template corresponding to the U5-PBS HIV-1 genomic RNA sequence; WT, wild type. A, D, E, F, I, L, M, R, T, V, W, and Y represent single-letter codes for Ala, Asp, Glu, Phe, Ile, Leu, Met, Arg, Thr, Val, Trp, and Tyr, respectively.

10.1021/bi026311z CCC: $22.00 © 2002 American Chemical Society
Published on Web 12/04/2002

with template nucleotides has been implicated in governing replication fidelity (*21*). This has been supported by recent evidence which demonstrates that substitutions in fingers and palm subdomains significantly alter the DNA binding affinity as well as fidelity of the enzyme (*22*−*27*). Our own investigations on residues constituting the dNTP binding pocket of HIV-1 RT led us to propose a model suggesting that recruitment of the correct versus incorrect nucleotides is governed by the flexibility of the substrate binding pocket, thereby directly influencing fidelity (*28*).

The structural and mechanistic aspects of HIV-1 RT infidelity appear to be intertwined with the complex phenomena of drug resistance. This is evidenced by the identification of a number of mutations that exhibit resistance to nucleoside inhibitors and also alter the nucleotide selectivity of HIV-1 RT (*22*, *23*, *28*−*34*). Analysis of the crystal structure of the HIV-1 RT−DNA−dNTP ternary complex has revealed that amino acid residues responsible for conferring sensitivity and/or resistance to nucleoside RT inhibitor (NRTI) are scattered on the palm and fingers subdomains (*7*, *29*, *35*, *36*) and interact with the incoming dNTP substrate either directly or via their interaction with neighboring residues (*20*). A number of structural elements have also been implicated as playing a key role in imparting drug resistance. For instance, a number of nucleoside analogue resistant mutations are located on the $\beta3-\beta4$ loop, the $\beta9-\beta10$ turn, and $\beta11$a/b regions of HIV-1 RT (*37*).

Non-nucleoside RT inhibitors (NNRTI) interact mainly in the $\alpha\beta$ sandwich hydrophobic pocket in the palm subdomain of the enzyme (*7*, *17*, *24*) as judged by the emergence of drug resistant variants carrying mutational changes in this region (*38*, *39*). Analysis of this region in the crystal structures of HIV-1 RT reveals the presence of a number of hydrophobic residues clustered between the structurally conserved $\alpha\beta\beta\alpha$ motif of the palm subdomain and at the junction of palm and fingers subdomains. Within the $\alpha\beta\beta\alpha$ motif, these residues include Ile-167, Leu-187, and Val-189, while Trp-153 lies adjacent to the conserved LPQG motif at the juncture of the palm and fingers subdomains. The exact significance of these residues is not known. Although Leu-187 and Val-189 are very close to the two essential catalytic residues (Asp-185 and Asp-186), their side chains are oriented in the opposite direction from Asp-185 and Asp-186 due to the secondary structure of the β-strand. The side chains of the relatively conserved residue Ile-167 and the highly conserved residues Leu-187 and Val-189 are buried in the hydrophobic core, though the precise significance of their distance from the catalytic center is not clear. Trp-153 resides on the loop between $\beta8$ and αE and is surrounded by a number of other hydrophobic residues within a radius of 4 Å, including Val-10, Thr-84, Leu-120, Phe-124, Pro-150, Phe-77, and Ile-159. Trp-153 together with these residues forms a strong hydrophobic core near the catalytic pocket.

In the study presented here, we have analyzed the contribution of the conserved hydrophobic residues Ile-167, Leu-187, Val-189, and Trp-153 in the catalytic function of RT. Although these residues do not form part of the NNRTI pocket per se, they are positioned such that any alteration in their side may influence the geometry of the NNRTI binding pocket via repositioning of the $\beta9$ and $\beta10$ strands harboring the catalytic aspartates. Interestingly, no naturally occurring mutations at these positions conferring the drug resistance phenotype have been reported, to date, though a conservative substitution at position 189 (Val → Ile) has been reported to emerge in HIV-1-infected cell cultures under selective pressure of a NNRTI, quinoxaline (*40*). We have carried out conserved and nonconserved amino acid substitutions at these positions and analyzed the resulting mutant enzymes, in the context of various biochemical characteristics such as efficiency of polymerization, ribonucleotide misincorporation, fidelity characteristics, resistance to nucleoside and non-nucleoside inhibitors, and steady state kinetic parameters. The significance of our findings is discussed in the context of the crystal structures of the enzyme.

EXPERIMENTAL PROCEDURES

Materials

Restriction endonucleases and DNA-modifying enzymes were obtained from Promega. HPLC-purified dNTPs, Sequenase, and DNA sequencing reagents were from Roche Molecular Systems, Inc. Expression vector pKK233, *Escherichia coli* expression strain JM109, and Fast Flow Chelating Sepharose (iminodiacetic-Sepharose) for immobilized metal affinity chromatography (IMAC) were obtained from Amersham Pharmacia Biotech. The ^{32}P-labeled dNTPs and ribonucleotides were the products of PrekinElmer Life Sciences. Synthetic template primers, sequencing primers, and mutagenic oligonucleotides were synthesized at the Molecular Resource Facility at the University of Medicine and Dentistry of New Jersey. HIV-1 RNA expression clone pHIV-PBS was a generous gift from M. A. Wainberg (*41*). All other reagents were of the highest available purity and were purchased from Roche Molecular Systems, Inc., Fisher, or Bio-Rad.

Methods

Expression of Plasmid Clones and in Vitro Mutagenesis. The recombinant plasmid pKK223-RT66 encoding p66 with metal binding hexahistidine (His tag) sequences at the N-terminal region was used as a template for mutagenesis and for expression and isolation of the wild-type homodimeric HIV-1 RT (*42*, *43*). For mutagenesis, two primers corresponding to sense and antisense strands containing the desired mutation were used to amplify pKK223-RT66 by high-fidelity PCR using the QuickChage Site-Directed Mutagenesis Kit from Stratagene. After the mutations at the desired positions had been ascertained by DNA sequencing, the mutant clones were expressed in *E. coli* strain JM109 and the enzymes isolated using IMAC columns as described previously (*31*). The purity of the proteins was assessed by SDS−PAGE. RT concentrations were determined using the Bio-Rad protein assay and normalized against known bovine serum albumin standards by densitometric scanning of the protein gel.

Preparation of the HIV-1 U5-PBS RNA Template. An HIV-1 RNA expression clone (pHIV-PBS) was used for the preparation of the U5-PBS HIV-1 genomic RNA template as described previously (*41*, *43*). The plasmid pHIV-PBS was linearized with *Acc*I and transcribed using T7 RNA polymerase. The transcription reaction was carried out using the enzyme, buffer, and rNTP solutions according to the manufacturer's protocol (Gibco-BRL).

Chart 1: Sequences of Heteropolymeric Template-Primers

1. U5-PBS HIV-1 RNA containing the primer binding site.

3'-CAG GGA CAA GCC CGC GGU GAC GAU CUC UAA AAG GUG UGA CUG AUU UUC CCA GAC UCC CUA GAG AUC AAU GGU CUC AGU GUG UUG UCU GCC CGU GUG UGA UGA ACU UCC UGA GUU CCG UUC GAA AUA ACU CCG AAU UCG UCA CCC AAG GGA UCA UCG GUC UCU CGA GGG UCC GAG UCU AGA -5'

2. 17-mer DNA PBS primer.

5' GTCCCTGTTCGGGCGCC-3'

3. Synthetic 30-mer RNA corresponding to U5-PBS RNA sequence.

3'-CAGGGACAAGCCCGCGGUGACGAUCUCUAA-5'

4. 30-mer DNA complementary to 30-mer U5-PBS RNA.

5'-GTCCCTGTTCGGGCGCCACTGCTAGAGATT-3'

5. 49-mer U5-PBS DNA template corresponding to U5-PBS sequence.

3'-CAGGGACAAGCCCGCGGTGACGATCTCTAAAAGG TGTGACTGATTTTCC-5'

6. 33-mer heteroplolymeric DNA template.

3'-GCA ATC GGT GAG GCT TCA CGG CAT ATT GCG CGT-5'

7. 21-mer dideoxy terminated primer corresponding to 33-mer DNA.

5'-CGT TAG CCA CTC CGA AGT GCC-3'

Polymerase Activity Assay. Polymerase activities of the wild-type and mutant enzymes were assayed on the heteropolymeric U5-PBS HIV-1 RNA and DNA templates. The nucleotide sequences of the heteropolymeric RNA and DNA templates and DNA primers are shown in Chart 1. Assays were carried out in a final volume of 50 μL containing 15 nM enzyme in 50 mM Tris-HCl (pH 7.8), 100 μg/mL bovine serum albumin, 5 mM $MgCl_2$, 1 mM dithiothreitol, 60 mM KCl, 100 nM template-primer, and 20 μM dNTPs containing [α-^{32}P]dCTP and [α-^{32}P]dGTP (0.5 μCi/nmol). Reactions were started by the addition of divalent metal ion, and the mixture was incubated at 37 °C for 5 min. Reactions were terminated by the addition of ice-cold 5% trichloroacetic acid containing 5 mM inorganic pyrophosphate (PP_i), and the acid insoluble radioactive material was collected on Whatman GF/B filters, dried, and counted for radioactivity in a Packard Tricarb liquid scintillation analyzer (*28*, *43*).

Template-Primer (TP) Binding Affinity. The dissociation constant (K_d) of the E−TP binary complexes of the wild-type HIV-1 RT and its mutant derivatives were determined in accordance with the procedure described by Astatke et al. (*44*). The heteropolymeric 33-mer DNA annealed to a 5′-^{32}P-labeled dideoxycytidine (ddC)-terminated 21-mer primer (0.3 nM) was incubated with varying concentrations of the individual enzyme proteins in a total volume of 10 μL containing 50 mM Tris-HCl (pH 7.8), 5 mM $MgCl_2$, and 0.01% BSA. Following incubation for 10 min at 4 °C, an equal volume of 2× gel loading dye containing 0.25% bromophenol blue and 20% glycerol was added to the mixture, and the resulting complexes were resolved on a 6% native polyacrylamide gel in Tris-borate buffer [85 mM Tris and 85 mM boric acid (pH 8.0)]. The amount of TP in the enzyme-bound form (E−TP binary complex) and in the free unbound form was determined by PhosphorImager analysis of the gel. The percent complexed DNA was plotted against enzyme concentration, and the $K_{d[DNA]}$ value was determined as the RT concentration at which 50% of the DNA is bound.

Stable Ternary Complex Formation Assay. Ternary complex (E−DNA−dNTP) formation was assessed according to the procedure described by Tong et al. (*45*). The wild-type enzyme and its mutant derivatives (10−50 nM) were incubated with 5′-^{32}P-labeled dideoxy-terminated 33-mer/21-mer template-primer (0.3 nM) in a total volume of 10 μL containing 50 mM Tris-HCl (pH 7.8), 5 mM $MgCl_2$, and 0.01% BSA to form the binary complexes (E−DNA). Ternary complex formation was achieved by incubating the binary complex in the presence of dNTP complementary to the next template nucleotide position (in this case dGTP, 200 μM). In each case, the concentration was chosen such that it resulted in a nearly complete shift during E−TP complex formation. To estimate the stability of the binary and ternary complex, a 300-fold molar excess of the same unlabeled template-primer (as trap) was added to the reaction mixture. After incubation for 10 min at 4 °C, 10 μL of 2× gel loading dye (0.25% bromophenol blue in 20% glycerol) was added and the complexes were resolved on a 6% native polyacrylamide gel followed by phosphorimaging. The bound E−TP−dNTP complex in each case was quantified using ImageQuant software.

Determination of the Apparent dNTP Binding ($K_{d[dNTP]}$). The apparent $K_{d[dNTP]}$ was determined using the procedure as described for stable ternary complex formation. In this experiment, the E−TP binary complexes of the WT enzyme and its mutant derivatives were allowed to form stable E−TP−dNTP ternary complexes in the presence of increasing concentrations of complementary nucleotide (dGTP, 0−4000 μM) at 4 °C for 10 min followed by addition of a 300-fold molar excess of DNA trap. The ternary complexes were resolved on a 6% native polyacrylamide gel followed by phosphorimaging. The labeled E−TP−dNTP complex and unbound free labeled TP were quantified using ImageQuant software. To determine the apparent $K_{d[dNTP]}$, the percent of total E−TP complex converted into stable E−TP−dNTP ternary complex as a function of dNTP concentration was fitted to the single-site ligand binding equation using Sigma Plot.

Steady State Kinetic Analysis of the Polymerase Reaction. The steady state kinetic parameters for WT HIV-1 RT and its mutant derivatives were determined on a heteropolymeric U5-PBS 49-mer/17-mer template-primer (100 nM). Reactions were carried out essentially as described for the polymerase activity assay except that the concentrations of dNTPs (2−150 μM) were varied and incubations were carried out at 37 °C for 10 min, so all reactions were within the linear time frame under these experimental conditions. The $K_{m(dNTP)}$ and V_{max} values were determined from a Lineweaver−Burk plot of the kinetic data, while $k_{cat(dNTP)}$ was determined from $V_{max}/[E]_{total}$.

Single-dNTP Exclusion Assay. The extent of misincorporation in the presence of three dNTPs was determined by extension of the 5′-^{32}P-labeled 17-mer primer annealed with a 2-fold molar excess of U5-PBS HIV-1 RNA and DNA templates. The reaction mixture contained 50 mM Tris-HCl (pH 7.8), 1 mM DTT, 0.1 mg/mL BSA, 5 mM $MgCl_2$, labeled template-primer (15 000 Cerenkov cpm/reaction), a three-dNTP mix (each at 50 μM), and mutant enzymes at varying concentrations (65−375 nM) exhibiting polymerase activity equivalent to 75 nM wild-type enzyme in a final volume of 5 μL. The reactions were carried out at room

temperature for 5 min and terminated by the addition of an equal volume of Sanger's gel loading dye (*46*). The reaction products were analyzed on a denaturing 8% polyacrylamide−8 M urea gel followed by phosphorimaging.

Primer Extension in the Presence of rNTP Substrates. The ability of the wild-type HIV-1 RT and its mutant derivatives to extend the primer by incorporating ribonucleotides was assessed on both heteropolymeric RNA and DNA templates primed with 5′-^{32}P-labeled 17-mer DNA primer as described previously (*28*). Reactions were also carried out in the presence of 50 μM dNTP substrates (control) or 500 μM rNTPs in a final volume of 5 μL at 25 °C for 10 min and terminated by the addition of an equal volume of Sanger's gel loading dye. The products were resolved by denaturing 8% polyacrylamide−8 M urea gel electrophoresis followed by phosphorimaging.

ddNTP Sensitivity of the Wild-Type Enzyme and Its Mutant Derivatives. The response to ddNTP was determined using U5-PBS HIV-1 RNA and DNA templates primed with 5′-^{32}P-labeled 17-mer PBS DNA primer. Wild-type and mutant enzymes (75 nM) were incubated with labeled template-5′-^{32}P-primer in a standard reaction mixture containing dNTP and ddNTP at a 1:1 ratio (200 μM each) in a final volume of 5 μL. The reactions were carried out at 37 °C for 30 min, terminated by the addition 5 μL of Sanger's gel loading dye (*46*), and resolved by denaturing 8% polyacrylamide−8 M urea gel electrophoresis followed by phosphorimaging.

Determination of the IC_{50} Value of Nevirapine. Wild-type or mutant enzymes (15−75 nM) were incubated at 4 °C for 5 min in the absence or presence of varying concentrations of nevirapine. The polymerase reactions were then carried out as described for the DNA-dependent DNA polymerase assay using 49-mer/17-mer as the template-primer. Percent polymerase activity was plotted as a function of individual nevirapine concentration. The IC_{50} value of nevirapine for each enzyme was determined by fitting the results from two independent experiments to a dose−response curve using nonlinear regression.

RESULTS

Construction and Purification of Mutant Enzymes. A total of 15 mutants of four amino acid residues at positions 153, 167, 187, and 189 in the polymerase subdomain of HIV-1 RT were generated and expressed in *E. coli*. The functional side chains of the target amino acid residues were either substituted with Ala or replaced with conserved or nonconserved residues. In some of the positions, the hydrophobic side chain was replaced with a polar uncharged or charged side chain. The enzyme proteins were purified to near homogeneity (>98% pure). The final purified protein was stored at −80 °C in 50% glycerol containing 50 mM HEPES (pH 7.0), 1 mM DTT, and 100 mM NaCl.

The studies presented here were performed with the homodimeric species (p66−p66) of the enzyme. To confirm that the results obtained with the homodimeric enzymes were similar with those obtained with the heterodimeric species, experiments involving the DNA binding affinity, stability of the E−DNA−dNTP ternary complex, and polymerase activity assays were repeated with the heterodimeric wild-type enzyme. The results obtained with both heterodimeric and homodimeric species were similar, suggesting identical biochemical properties. This is consistent with previously reported data (*9*).

Table 1: Polymerase Activity of Wild-Type HIV-1 RT and Its Mutant Derivatives[a]

enzyme	U5-PBS DNA/17-mer DNA template-primer	U5-PBS RNA/17-mer DNA template-primer
WT	100	100
W153A	27 ± 4.5	30 ± 5.0
W153F	90 ± 11.4	78 ± 7.2
W153Y	42 ± 5.1	58 ± 5.6
I167A	29 ± 3.3	39 ± 4.6
I167D	84 ± 10.7	76 ± 8.2
I167L	20 ± 3.7	30 ± 4.4
I167T	134 ± 13.2	118 ± 8.9
I167V	30 ± 5.4	46 ± 3.5
L187A	24 ± 3.6	40 ± 3.6
L187I	71 ± 8.6	54 ± 6.6
L187R	80 ± 9.8	79 ± 8.0
L187V	78 ± 9.9	101 ± 12.8
V189A	137 ± 14.1	98 ± 9.2
V189I	125 ± 10.8	100 ± 11.0
V189M	127 ± 12.6	90 ± 8.6

[a] The polymerase activities of WT HIV-1 RT and its mutant derivatives were determined using each enzyme (15 nM) on two different template-primers in the presence of Mg^{2+} as the divalent cation as described in Experimental Procedures**.** The values represent the percent activity of the wild-type enzyme and are the mean values ± the standard deviation of three independent experiments.

DNA Polymerase Activity of Wild-Type (WT) HIV-1 RT and Its Mutant Derivatives. The DNA- and RNA-dependent DNA polymerase (DDDP and RDDP) activities of wild-type HIV-1 RT and its mutant derivatives were examined on heteropolymeric RNA and DNA templates, and the results were expressed as the percent of WT activity (Table 1). Of the three mutants of Trp-153, the polymerase activity of the W153Y mutant carrying an aromatic ring with a polar OH group was decreased by approximately 50%, while W153F with the nonpolar hydrophobic side chain retained near-wild-type activity. In contrast, replacing the Trp side chain with Ala registered an approximately 70% loss of polymerase activity on all templates. Similarly, all three mutants of Ile-167 with a smaller side chain (Ile → Ala) or substituted with a similar hydrophobic side chain (Ile → Leu and Ile → Val) exhibited a 54−80% reduction in polymerase activity. However, substitution with a polar and uncharged side chain at this position (Ile → Thr) enhanced the polymerase activity by approximately 18 and 34% on RNA and DNA templates, respectively, while substitution with a charged side chain (Ile → Asp) retained 76−84% of the WT polymerase activity. These data suggest that the hydrophobic nature of the side chain of Ile at position 167 is not critical since substitution with polar or charged side chains at this position either enhanced or retained the near-wild-type activity of the enzyme. However, it is intriguing that substitution of a conserved side chain of either Leu or Val has a negative impact on the enzyme activity.

Among the four mutant derivatives of Leu at position 187, L187A displayed a 60−76% reduction in the polymerase activity while other mutants carrying either a nonpolar conservative substitution (L187I and L187V) or a charged side chain (L187R) displayed a marginal decrease in their activities compared to the wild-type enzyme. Interestingly, all the mutant derivatives of Val-189 displayed enhanced polymerase activity (125−137% of WT activity) on the DNA

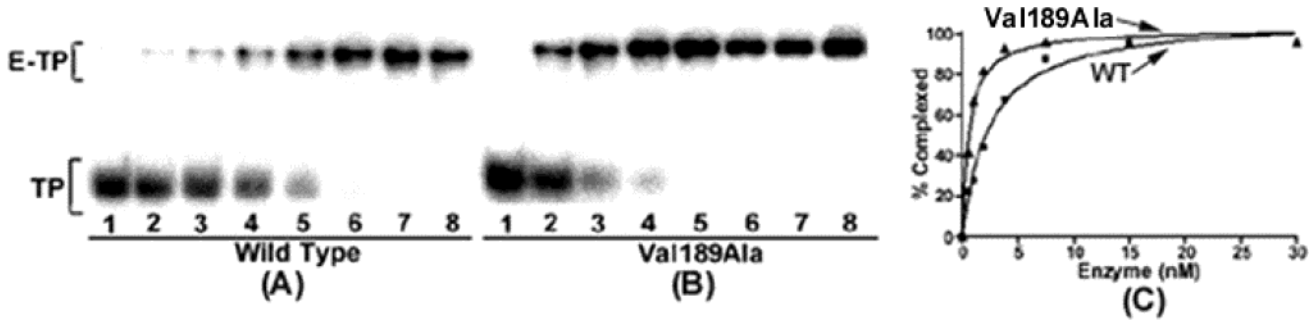

FIGURE 1: Gel mobility shift assay for analysis of DNA binding affinity. The 33-mer DNA primed with the 5′-^{32}P-labeled dideoxycytidine (ddC)-terminated 21-mer DNA primer was incubated with varying concentrations of the individual enzyme at 4 °C for 10 min. The mixture was electrophoresed under nondenaturing conditions on a 6% (w/v) polyacrylamide gel and analyzed on a PhosphorImager. Panels A and B represent the gel shift patterns obtained with the wild-type enzyme and the Val189Ala mutant, respectively. Lanes 1−8 show the formation of the E−TP complex in the presence of protein concentrations of 0.0, 0.47, 0.94, 1.88, 3.75, 7.5, 15, and 30 nM (wild type, panel A) and 0.0, 0.24, 0.47, 0.94, 1.88, 3.75, 7.5, and 15 nM (Val189Ile, panel B), respectively. The positions of the free template-primer (TP) and enzyme-bound template-primer (E−TP binary complex) are indicated on the left. The percent of E−TP complex formed as a function of enzyme concentration (C) was plotted for determining the K_d value of the individual enzyme.

template while retaining wild-type activity on the RNA template. These data suggest that substitution at position 187 may impact the catalytic activity of the enzyme on both DNA and RNA templates while substitution at position 189 stimulates the DNA-dependent polymerase activity. Although the side chains of Leu-187 and Val-189 are oriented in a direction opposite from the catalytic Asp-185 and Asp-186, their hydrophobic side chains may influence the flexibility of the catalytic pocket.

DNA Binding Affinity of the Mutant Enzymes. Since the mutant derivatives of Trp-153, Ile-167, Leu-187, and Val-189 displayed either enhancement of or a reduction in the polymerase activity, it may be assumed that the modulation of their activity may be linked to an alteration in their DNA binding affinity. To ascertain this possibility, we determined the equilibrium dissociation constant (K_d) of the E−TP binary complex for the wild-type enzyme and its mutant derivatives with a gel mobility shift assay. For this purpose, we used a 33-mer heteropolymeric DNA template primed with 5′-^{32}P-labeled dideoxy-terminated 21-mer DNA. Figure 1 depicts a typical gel retardation analysis of the E−TP complex formed in case of the wild-type enzyme and Val189Ala mutant.

The results listed in Table 2 (column 2) clearly indicate that enhancement of the polymerase activity observed with the mutant derivatives of Val-189 correlates with an increase in their TP binding affinity. The $K_{d[DNA]}$ values for Val-189 mutants ranged from 0.4 to 0.6 nM versus 2.4 nM for the wild-type enzyme. The K_d value for the I167T mutant (0.2 nM) was 12-fold lower than that of the wild-type enzyme which may explain its increased polymerase activity versus that of the wild-type enzyme. However, a marginal increase (∼2-fold) in $K_{d[DNA]}$ was observed with the W153A mutant, while a 2-fold lower $K_{d[DNA]}$ was noted with the W153F mutant. These observations account for the polymerase activity profiles of the Trp-153 mutants (Table 1). The less active mutant derivatives of Ile-167 (I167L and I167V) also exhibited a 2.7−5.2-fold reduction in their DNA binding affinity. In contrast, replacement of Ile with a polar uncharged side chain of Thr at position 167 enhanced the DNA binding affinity by 12-fold which may account for the enhanced polymerase activity observed with this mutant. The DNA binding affinity of two other mutants, Ile167Asp and Ile167Ala, was marginally increased (1.6-fold) with either no change (Ile → Asp) or reduced polymerase activity (Ile → Ala). No significant correlation between DNA binding affinity and polymerase activity was observed with the mutant derivatives of Leu-187. Substitution of Leu with Ala at position 187 resulted in no increase in the affinity for DNA with a 4-fold decrease in the polymerase activity, whereas other mutant derivatives with approximately 1.1−2.3-fold higher $K_{d[DNA]}$ values displayed no significant change in polymerase activity. These observations suggest that the change in the polymerase activity of some of the mutants of these hydrophobic residues is not related to their DNA binding ability.

Table 2: Values of $K_{d[DNA]}$ and Apparent $K_{d[dNTP]}$ for Wild-Type HIV-1 RT and Its Mutant Derivatives[a]

	dissociation constant of the E−TP binary complex		apparent dNTP binding affinity	
enzyme	$K_{d[DNA]}$ (nM)	mutant/WT ratio	$K_{d[dNTP]}$ (μM)	mutant/WT ratio
WT	2.4	−	12.0	−
W153A	4.2	1.8	54.0	4.5
W153F	1.2	0.5	3.8	0.3
W153Y	3.2	1.3	50.0	4.2
I167A	1.5	0.6	301.0	25.1
I167D	1.5	0.6	31.6	2.6
I167L	6.5	2.7	218.0	18.2
I167T	0.2	0.1	3.0	0.3
I167V	12.4	5.2	335.0	27.9
L187A	1.8	0.8	141.0	11.8
L187I	5.5	2.3	50.0	4.2
L187R	2.7	1.1	56.0	4.7
L187V	5.2	2.2	39.0	3.3
V189A	0.5	0.2	5.6	0.5
V189I	0.4	0.2	1.6	0.1
V189M	0.6	0.3	7.3	0.6

[a] The $K_{d[DNA]}$ in the binary complex and the apparent $K_{d[dNTP]}$ in the ternary complex for the wild-type HIV-1 RT and the individual mutants were determined by a gel mobility shift assay using a 5′-^{32}P-labeled dideoxy-terminated 33-mer/21-mer DNA template-primer. The percent of template-primer associated in the binary and ternary complexes was quantified using ImageQuant software. The values of $K_{d[DNA]}$ and apparent $K_{d[dNTP]}$ are averages of two independent determinations.

Ternary Complex Formation by Wild-Type and Mutant Enzymes. In the crystal structures of the ternary complex of HIV-1 RT (E−DNA−dNTP), a significant movement of subdomains in the polymerase cleft has been noticed upon

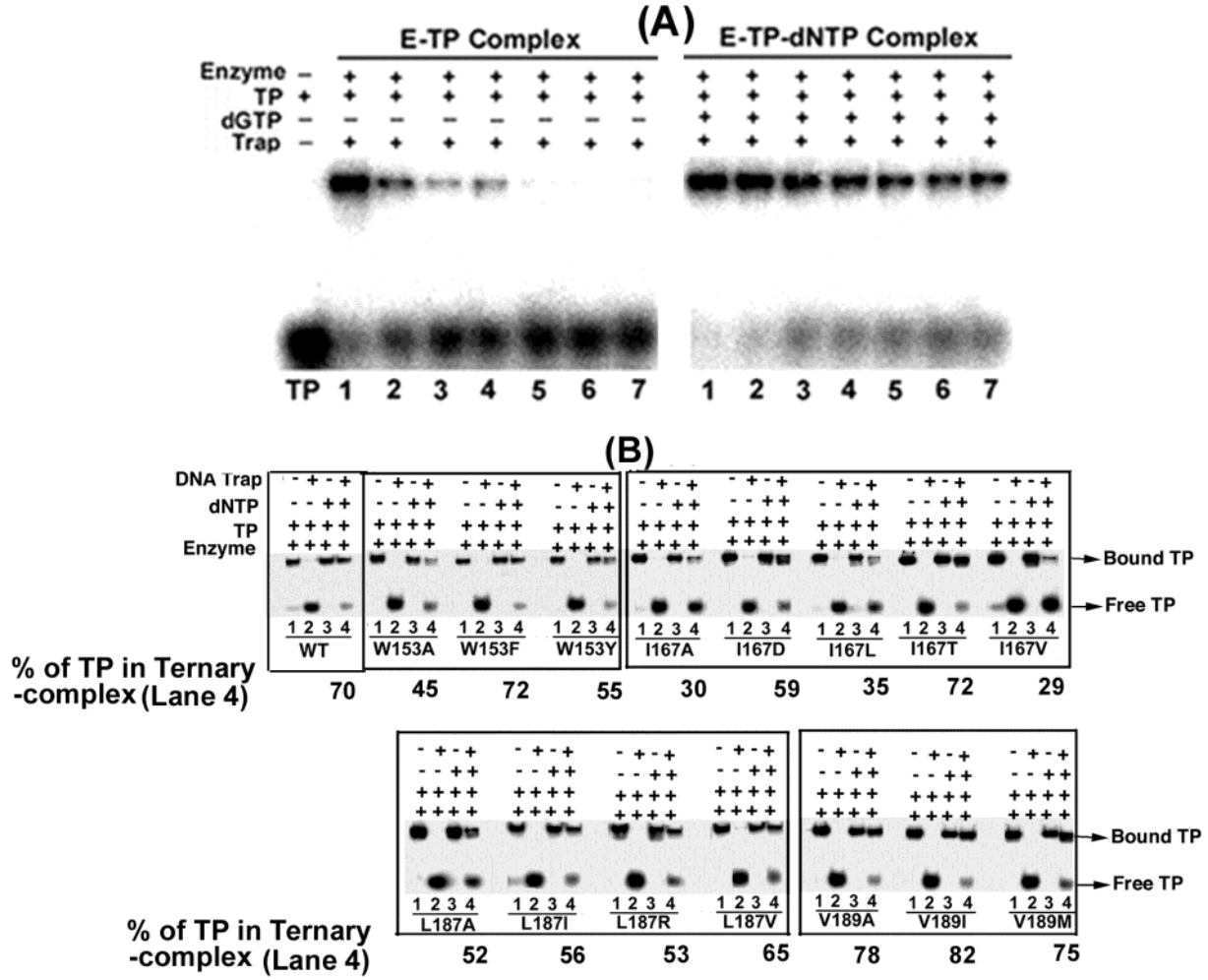

FIGURE 2: (A) Effect of DNA trap concentration on the formation of E−TP and E−TP−dNTP complexes. The binary complex (left panel) and ternary complex (right panel) of the WT enzyme were formed by incubating 15 nM enzyme protein with radiolabeled ddC-terminated TP (33-mer/21-mer, 0.3 nM) at 4 °C for 10 min in the absence or presence of complementary dNTP (dGTP, 200 μM). The individual complex that formed was competed out by addition of increasing concentrations of the DNA trap. Lanes 1−7 represent trap concentrations of 0, 3, 15, 30, 50, 75, and 100 nM, respectively. It may be noted that the ternary complex that formed is resistant to competition by DNA trap. This suggests that the ternary complex is more stable than the binary complex. (B) Analysis of the ternary complex formed by the mutant derivatives of HIV-1 RT. The binary (lane 1) and ternary complex (lane 3) formed by the individual mutant enzymes as described for panel A were challenged by addition of DNA trap (100 nM) to determine their stabilities and analyzed on a nondenaturing polyacrylamide gel. Lanes 2 and 4 show the extent of dissociation of the template-primer in the binary and ternary complex, respectively. The numbers at the bottom indicate the percent of undissociated TP in the ternary complex.

dNTP binding (*20*). The fingers subdomain in the E−DNA complex moves 20 Å toward the palm subdomain (fingers closing). Under fingers closing conditions following dNTP binding, the DNA in the E−DNA binary complex is locked in a stable ternary complex poised for catalysis. An in vitro assay using a dideoxy-terminated primer annealed with the template has recently been reported which allows the next correct dNTP to bind in the ternary complex without it being incorporated (*45*). We have used this assay system to assess the ability of various mutant enzymes to form the ternary complex. Since binding of dNTP to the enzyme is an ordered mechanism which occurs only after DNA binding, the extent of labeled DNA remaining bound to the enzyme in the presence of dNTP and DNA trap represents the level of ternary complex that is formed. These results are presented in Figure 2. In the case of the wild-type enzyme, it was observed that the E−TP binary complex was completely competed out by a more than 300-fold molar excess of DNA trap (Figure 2A, left panel). In contrast, a significant amount of the E−TP binary complex converted to the E−TP−dNTP ternary complex was resistant to competition with DNA trap (Figure 2A, right panel), suggesting the stability of the ternary complex.

Using these experimental conditions, we evaluated the formation of a stable ternary complex by the mutant enzymes (Figure 2B). Like the wild-type enzyme, the E−TP binary complexes (lane 1) formed by mutant derivatives of the four hydrophobic residues were effectively competed out by DNA trap (lane 2). In the presence of the incoming complementary dNTP, the labeled TP bound to the enzyme representing the putative ternary complex (lane 3) was resistant to competition by DNA trap (lane 4). The mutant derivatives indicating enhanced enzyme activity (I167T and Val-189 mutants) exhibited an increased extent of ternary complex formation (102−116%), while mutant derivatives with decreased enzyme activity (W153A, W153Y, I167A, I167L, I167V, and L187A) exhibited lower extents of ternary complex formation (42−78%) than the wild type. Mutant enzymes showing near-wild-type activity (W153F, I167D, L187I,

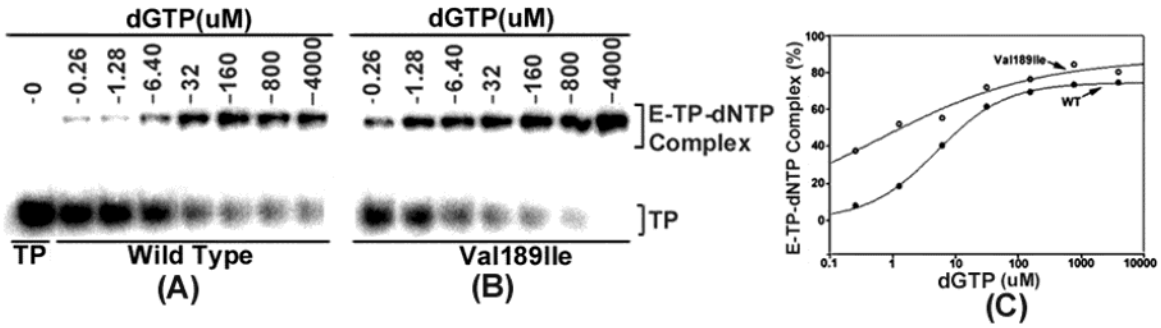

FIGURE 3: Determination of the dNTP binding affinity in the ternary complex by gel shift analysis. The binding affinities [$K_{d(dNTP)}$] of the wild-type enzyme and its mutant derivatives in the ternary complex were determined by incubating the individual E−TP binary complex at different concentrations of dNTP substrates and subjecting them to gel shift analysis. Panels A and B show ternary complex formation by the wild type and Val189Ile mutant, respectively, at varying dNTP concentrations. The positions of the template-primer (TP) in free form as well as in the ternary complex are indicated on the right. The dNTP binding affinity ($K_{d[dNTP]}$) in the ternary complex for the wild-type enzyme and Val189Ile mutant (C) was determined by quantifying the percent E−TP−dNTP complex formation as a function of increasing concentrations of complementary dNTP (dGTP in this case) and fitting the data to the equation for single-site ligand binding using Sigma Plot.

L187R, and L187V) displayed 75−96% stable ternary complex formation compared to the wild-type enzyme.

Apparent dNTP Binding Affinity. Since the mutants formed varying amounts of the E−TP−dNTP complex, we also determined their apparent dNTP binding affinity (apparent $K_{d[dNTP]}$) by analysis of the stable ternary complexes. Representative data showing gel retardation analysis of E−TP−dNTP complex formation with the wild-type enzyme and Val189Ile mutant enzyme are shown in Figure 3. A curve of the percent ternary complex formed versus dNTP concentration was plotted using Sigma Plot software (Figure 3C). Using this technique, the apparent $K_{d[dGTP]}$ value obtained for wild-type RT was 12 μM. The $K_{d[dATP]}$ value determined by pre-steady state burst analysis has been reported to be in the range of 2.4−4 μM (*47*, *48*). These variations in $K_{d[dNTP]}$ may be due to the difference in nucleotide substrate and experimental procedures and/or conditions. Further, results shown in column 3 of Table 2 clearly indicate the correlation between the polymerase activity of the mutant enzymes and their binding affinities for dNTPs. The mutants showing higher polymerase activity also displayed increased apparent dNTP binding affinities and vice versa with the sole exception of Phe-153.

Steady State Kinetic Analysis of the Mutant Enzymes. To determine whether alteration in the apparent dNTP binding affinity of these mutants is consistent with their kinetic parameters, we determined their steady state kinetic parameters (Table 3). Mutant derivatives of Ile-167 with decreased apparent dNTP binding affinity displayed higher K_m values for the dNTP substrate, suggesting that the decreased polymerase activity may be due to alteration in their dNTP binding pocket. In contrast, highly active mutant derivatives such as I167T, V189A, V189I, and V189M showing enhanced DNA and apparent dNTP binding affinities exhibited 3−7-fold higher catalytic efficiency, suggesting that increases in both the TP and dNTP binding affinities are the prime factors for improved catalytic efficiency. However, less active mutant derivatives of Trp-153 and Leu-187 with decreased DNA and dNTP binding affinities showed no significant change in $K_{m(dNTP)}$, suggesting that the perturbation in DNA binding by these mutations may be the main factor for reduction in their catalytic efficiency. The L187A mutant with no significant increase in DNA binding affinity but an 11.8-fold decrease in the apparent dNTP binding affinity also displayed a 9-fold higher $K_{m\ (dNTP)}$. These results suggest a possible defect in the formation of the stable ternary complex.

Table 3: Steady State Kinetic Constants for Wild-Type HIV-1 RT and Its Mutant Derivatives[a]

enzyme	$K_{m[dNTP}$ (μM)	k_{cat} (s^{-1})	k_{cat}/K_m ($\times 10^3\ s^{-1}\ M^{-1}$)	mutant/WT ratio of k_{cat}/K_m
WT	5.9	0.132	22.4	1
W153A	9.4	0.082	8.8	0.40
W153F	9.7	0.208	21.5	0.96
W153Y	9.7	0.108	11.1	0.50
I167A	87.5	0.052	0.6	0.03
I167D	31.3	0.072	2.3	0.10
I167L	54.0	0.056	1.0	0.05
I167T	2.0	0.144	72.0	3.21
I167V	67.8	0.027	0.4	0.02
L187A	54.0	0.035	0.7	0.03
L187I	10.9	0.092	8.4	0.38
L187R	8.5	0.096	11.3	0.51
L187V	9.6	0.088	9.2	0.41
V189A	4.9	0.684	139.6	6.23
V189I	4.9	0.736	150.2	6.71
V189M	6.8	0.676	99.4	4.44

[a] The steady state kinetic parameters for wild-type HIV-1 RT and its mutant derivatives were analyzed on the heteropolymeric 49-mer/17-mer DNA template-primer and Mg^{2+}-dNTP substrates at 37 °C as described in Experimental Procedures. The values are averages of three independent experiments.

Misinsertion and/or Mispair Extension by Mutant Derivatives of HIV-1 RT. Since the primer terminus and template nucleotide are constituents of the dNTP-binding pocket, any alteration in their binding to the enzyme is expected to influence their ability to incorporate the correct nucleotide. It was, therefore, of interest to ascertain if these mutant derivatives with varying DNA and dNTP binding affinities exhibited any change in their preference for correct or incorrect nucleotides. Experiments were therefore carried out to assess the extent of mismatch synthesis and its extension by all 15 mutant derivatives and compare them with those of the WT enzyme. The results depicted in Figure 4 demonstrate substantial accumulation of DNA products at the sites preceding the missing nucleotide in all the reactions. A significant portion of the accumulated products was further extended to longer products due to misinsertion and subsequent extension, the magnitude of which varied depending

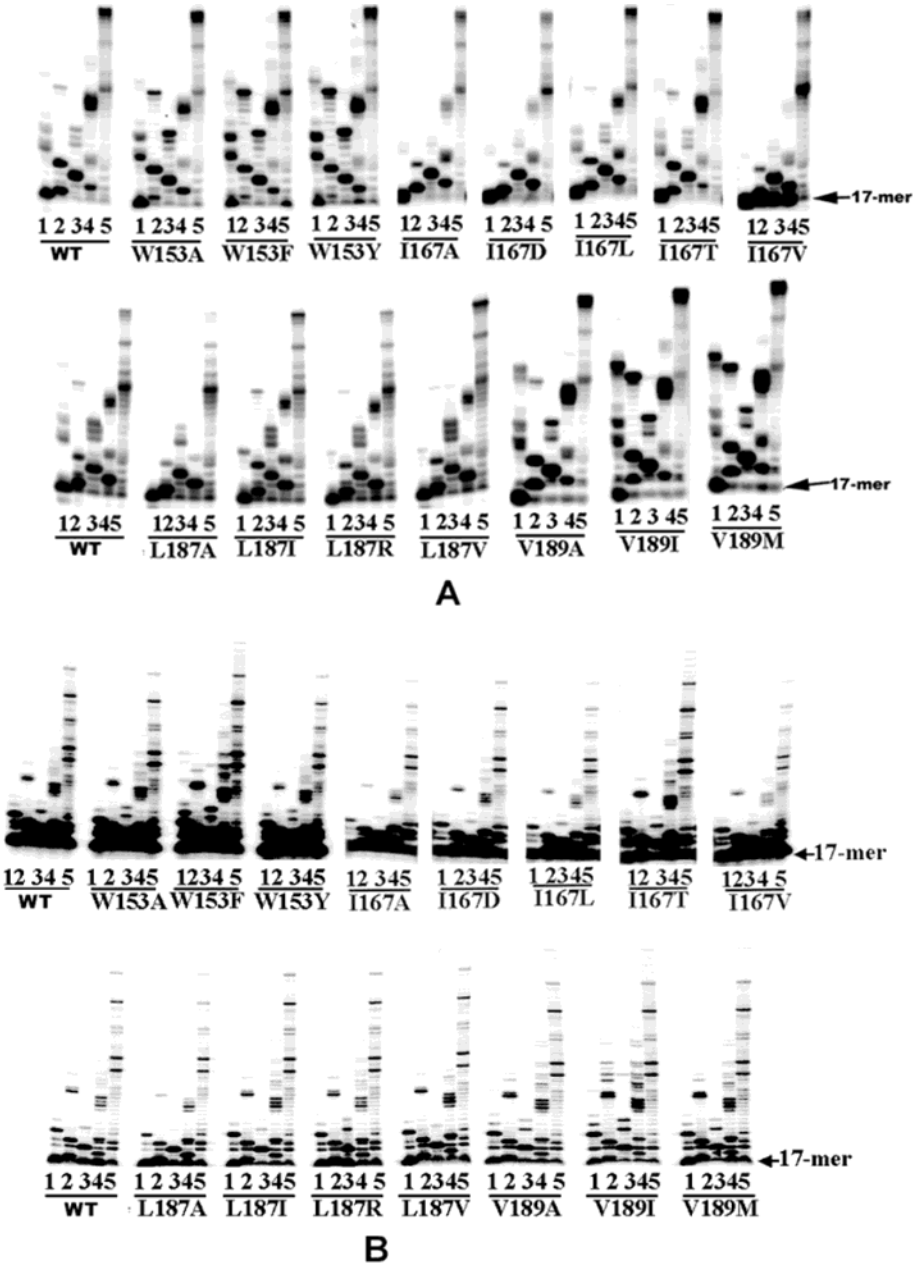

FIGURE 4: Misincorporation and mispair extension catalyzed by WT HIV-1 RT and its mutant derivatives. The U5-PBS 49-mer DNA (A) and RNA (B) templates primed with 5′-^{32}P-labeled 17-mer PBS primer were used to assess the extent of misinsertion and mispair extension. The concentration of the mutant enzyme was normalized to obtain activity equivalent to that of the wild-type enzyme. The final enzyme concentrations were as follows: 75 nM wild-type enzyme and W153F, I167D, and I167T mutants, 65 nM Val-189 mutant derivatives, 100 nM L187I, L187R, and L187V, 175 nM W153Y, 250 nM I167V, 300 nM W153A, I167A, and L187A, and 375 nM I167L. Reactions were carried out for 5 min at 25 °C in the presence of only three dNTPs, and the products were analyzed by denaturing PAGE followed by phosphorimaging. Lanes 1−4 represent reactions carried out in the absence of dATP, dCTP, dGTP, and dTTP, respectively, from the dNTP mix in the respective set of experiments. Lane 5 represents the reactions carried out in the presence of all four dNTPs (50 μM each).

on the enzyme and the nature of the template. Different patterns of mispair synthesis and extension were observed on DNA (Figure 4A) and RNA templates (Figure 4B). All the mutant derivatives of Ile-167 and Leu-187 displayed a pattern similar to that of the wild type or somewhat improved fidelity in comparison to the WT RT. In contrast, all the mutant derivatives of Trp-153 and Val-189 were more error prone than the wild-type enzyme on both DNA and RNA templates. While the DNA binding affinity and the misinsertion and/or mispair extension synthesis catalyzed by the mutant enzymes appear to be unrelated, some correlation exists between the apparent dNTP binding affinity and misinsertion and/or mispair extension ability of the enzymes. Other than two mutants of Trp-153 (W153A and W153Y) and one mutant of Ile-167 (I167T), all other mutants with increased apparent dNTP binding affinity were more error prone than the wild-type enzyme. The other mutants with decreased dNTP binding affinity were either less error prone or similar to the wild-type enzyme.

Ability To Incorporate rNTP and ddNTP Substrates. The variable misinsertion and mispair extension pattern observed with the above-mentioned mutant derivatives prompted us to examine their abilities to discriminate between rNTPs, ddNTPs, and dNTPs. In the case of the error prone mutants, with the exception of W153F and V189I which exhibited higher levels of incorporation of rNTPs on both DNA and

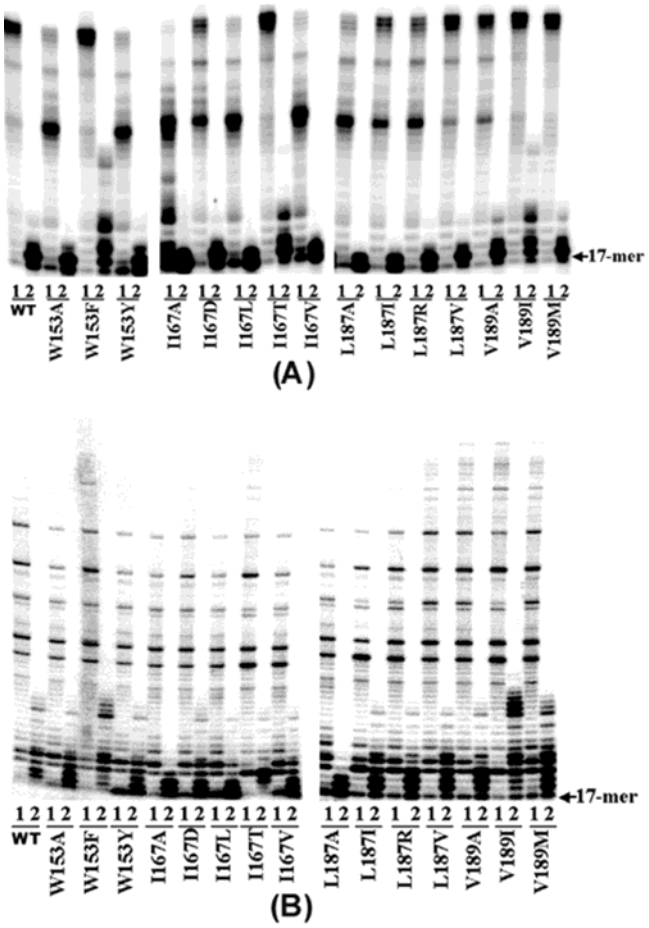

FIGURE 5: Utilization of rNTP substrates by WT HIV-1 RT and its mutant derivatives. The ability of the WT enzyme and its mutant derivatives to incorporate rNTPs and dNTPs was assessed on both 49-mer U5-PBS DNA (A) and RNA (B) templates primed with 5′-^{32}P-labeled 17-mer DNA primer. Lanes 1 and 2 represent reactions carried out in the presence of all four dNTPs and rNTPs, respectively.

RNA templates, the other mutants exhibited a wild-type rNTP incorporation pattern (Figure 5). Of the four less error prone mutants, I167D exhibited an rNTP incorporation pattern similar to that of the WT enzyme. In contrast, I167A and L187A exhibited lower levels of incorporation on both RNA and DNA templates, whereas I167V discriminated against rNTPs specifically on a DNA template (Figure 5A).

Examination of the sensitivities of these 15 mutant RTs to ddNTPs (Figure 6) revealed that with the exception of six mutants (W153A, W153F, W153Y, I167T, L187R, and I167D) which were more sensitive than the wild-type RT on the DNA template (Figure 6A), all others displayed wild-type RT sensitivity on both RNA and DNA templates (data not shown). These results suggest that any point mutation at these positions may potentially affect viral replication.

Sensitivity to Non-Nucleoside RT Inhibitor (NNRTI). Since the NNRTI binding pocket is constituted by hydrophobic residues in the palm subdomain, it was of interest to examine the sensitivity of these conserved hydrophobic residues for a NNRTI, nevirapine. The results shown in Figure 7 indicate that all the nonconservative mutations of these residues yielded enhanced sensitivity to nevirapine. Interestingly, conservative mutants also either exhibited increased sensitivity or were similar to the wild-type enzyme. These results suggest that mutations at these positions in RT enhance the hypersensitivity of the virus to NNRTI. This may well explain why the virus does not select for mutations at these positions in response to drug therapy.

DISCUSSION

In the study presented here, we have probed the functional significance of Trp-153, Ile-167, Leu-187, and Val-189, four hydrophobic residues in the structurally conserved $\alpha\beta\beta\alpha$ motif of the palm subdomain of HIV-1 RT in the context of the enzyme structure. In the three-dimensional structure of HIV-1 RT, Trp-153 is surrounded by a number of hydrophobic residues within a 4 Å radius, including Val-10, Phe-124, Asn-81, Leu-120, Phe-77, Pro-150, Pro-157, and Ile-159. Trp-153 together with these residues forms a strong hydrophobic core near the catalytic pocket. Isoleucine 167 is located on the αE helix in the palm subdomain which contains two other important residues, Phe-160 and Gln-161, that have been implicated in conferring fidelity and AZT susceptibility to the enzyme, respectively (*49*, *50*). The main chain oxygen of Ile-167 also makes hydrogen bond contact with the nitrogen atom of His-208 in addition to hydrophobic interactions with Trp-212, Leu-209, and Leu-214. A naturally occurring mutation (His → Tyr) at position 208 has been shown to confer the phosphono-formate resistance phenotype to HIV-1 (*51*). Leu-187 and Val-189 residing on the β10 sheet interact with each other and are surrounded by residues Leu-205, Leu-209, Ile-180, Ile-178, Leu-109, and Ile-202.

Although the side chains of these residues do not interact directly with the residues in the catalytic pocket, conservative or nonconservative substitutions at these positions substantially influence the polymerase function of the enzyme and corresponding kinetic parameters (Tables 1−3). For instance, substitution at position 189 (Val → Ala, Ile, or Met) significantly enhances the affinity of the enzyme for DNA and dNTP in both the binary and ternary complexes (Table 2), while the opposite effect was observed upon substitution at position 187 (Leu → Ile, Arg, or Val). All the mutant derivatives of Val-189 exhibited increases in polymerase activity, albeit with relatively improved misinsertion and mispair extension abilities (Figure 4). Our activity data with mutant derivatives of Val-189 (V189A and V189I) and Ile-167 (I167T) are in contradiction with an earlier report on these mutants by Wrobel et al. (*52*). This is not surprising since the substantially lower activities reported with Val189Ala, Val189Ile, and Ile167Thr mutants may be accounted for by the negligible extent of expressions or stabilities of these proteins as detected by Western blot analysis of the crude cell lysates (*53*).

In HIV-1 RT, a distinct hydrophobic pocket is formed upon binding of the non-nucleoside inhibitor. This pocket is close to the β9−β10 hairpin in the palm subdomain of p66 that contains two of the three catalytic aspartate residues in the highly conserved YMDD motif (*7*). The pocket is formed by residues on β6, β9, and β10 on one side and residues on β12−β14 on the other side. Leucine 187 and valine 189 located on β10 are constituents of the hydrophobic pocket, although they do not have direct contact with the NNRTI. Although Val-189 has not been directly implicated in binding to non-nucleoside inhibitors of HIV-1 RT (NNRTI), Val → Ile substitution at this position has been

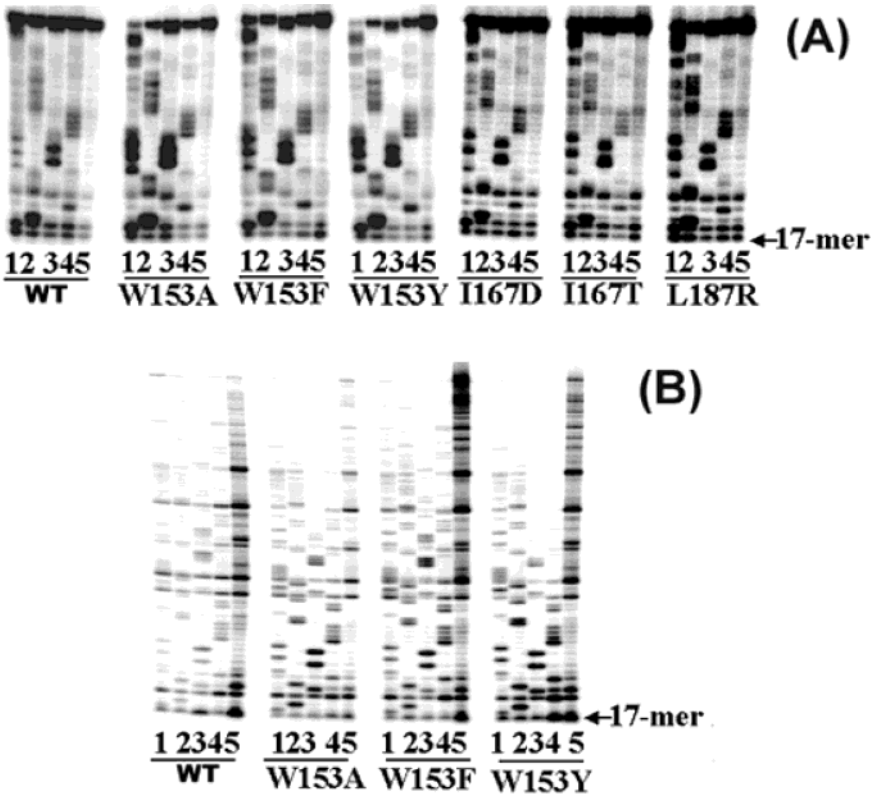

FIGURE 6: Sensitivity of WT HIV-1 RT and its mutant derivatives to dideoxyribonucleoside triphosphates. The U5-PBS 49-mer DNA (A) and RNA (B) templates primed with the 5′-^{32}P-labeled 17-mer PBS primer were used to analyze the sensitivity of the individual enzymes to ddNTPs. The ratio of dNTP to ddNTP in the reaction mixture was equimolar. Reactions were carried out for 30 min at 37 °C, and the products were resolved on an 8% denaturing polyacrylamide−urea gel followed by phosphorimaging. Lanes 1−4 represent the reactions carried out in the presence of ddATP, ddCTP, ddGTP, and ddTTP, respectively. Lane 5 represents the control reactions in the absence of ddNTPs. The position of the 17-mer primer is denoted on the right.

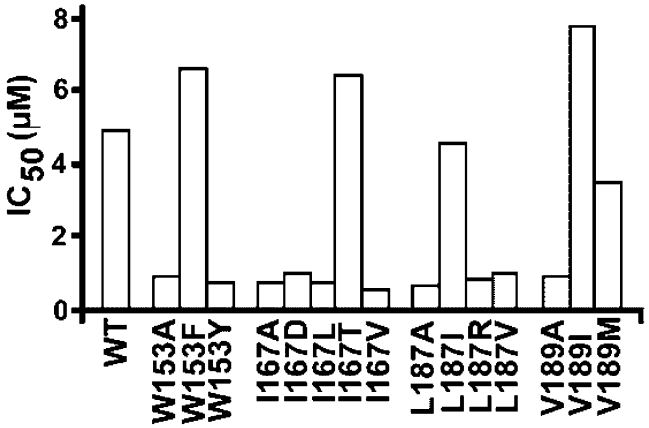

FIGURE 7: Sensitivity of WT HIV-1 RT and its mutant derivatives to nevirapine. The sensitivity of the wild-type RT and its mutant derivatives to nevirapine was analyzed on U5-PBS 49-mer/17-mer template-primer as described in Experimental Procedures. The IC_{50} value of the inhibitor for each enzyme was determined from the plot of the percent polymerase activity versus nevirapine concentration as described in Experimental Procedures. The values shown are an average of two independent experiments.

reported in vitro in response to quinoxaline, a NNRTI (*40*). Our results with the V189I mutant indicate no significant change in the sensitivity to nevirapine, while a 5-fold increase in sensitivity was noted with the nonconservative V189A mutant.

Trp-153, a constituent of motif B in retroviral RTs, is located next to the highly conserved LPQG motif on the β8−αE loop at the junction of the finger and palm subdomains of HIV-1 RT. Glutamine 151 of this motif is a crucial residue implicated in dNTP binding and ddNTP sensitivity (*25*, *26*, *54*). Glycine 152, a residue preceding Trp-153, interacts with the template base; a substitution (Gly → Ala) at this position completely inactivates the enzyme (*55*, *56*). Trp-153 is conserved in reverse transcriptases from Rous sarcoma virus, mouse mammary tumor virus, visna virus, Mason-Pfitzer monkey virus, and Caprine arthritis encephalitis virus. In some of the retroviral RTs such as Moloney murine leukemia virus, HTLV-I, HTLV-II, equine infectious anemia virus, and bovine leukemia virus, Phe is found in place of Trp. In our studies, Trp → Phe substitution at this position in HIV-1 RT did not alter the polymerase activity of the enzyme (Table 1). These observations suggest that the side chain of Phe at position 153 offers the same advantage to the enzyme as Trp in the wild-type enzyme. Surprisingly, another conservative Trp → Tyr substitution at this position was not favorable as it reduced the binding affinity for dNTP in the ternary complex.

In the crystal structure of the ternary complex (*20*), the bulky hydrophobic side chain of Trp-153 is positioned between the two template interacting residues, Gly-152 and Lys-154, and may possibly influence the geometry of the catalytic site. Trp-153 is at the center of the hydrophobic core, at the junction of the palm and fingers subdomains in the vicinity of the catalytic center (Figure 8A). Additional interactions of Trp-153 within a 4 Å radius are seen with Ser-156 and Phe-77 (Figure 8A), of which Ser-156 is

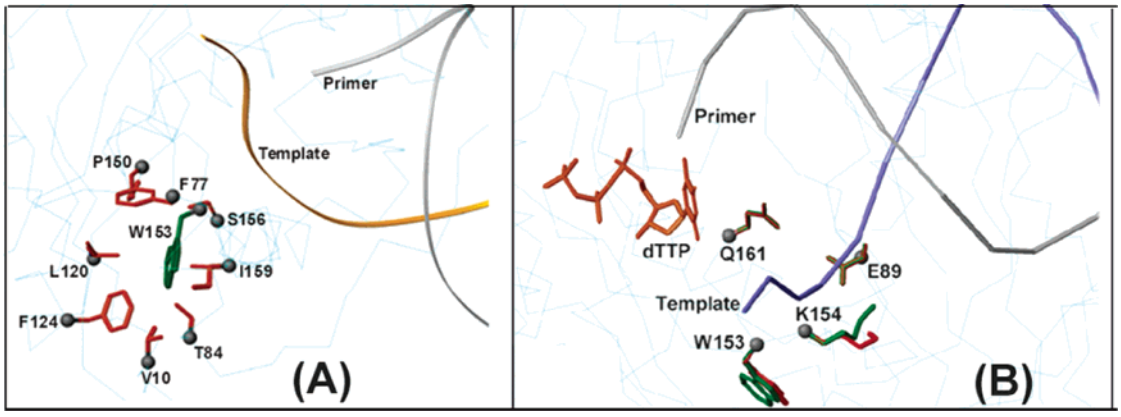

FIGURE 8: (A) Hydrophobic core at the base of fingers subdomain of HIV-1 RT. The position of Trp-153 and hydrophobic residues in its vicinity forming a hydrophobic core located between the fingers and palm at the base of fingers is as shown in panel A. The amino acids displayed here are from the ternary complex crystal structure of HIV-1 RT (PDB entry 1rtd). Also shown are two nonhydrophobic residues, Ser and Thr, the aliphatic groups of which face the hydrophobic core. (B) Effect of mutation of Trp-153 on the network of interactions mediated by Lys-154. Mutant modeling was performed using Look version 3.5 (Molecular Application Group). In the wild-type enzyme, Lys-154 forms a salt bridge with Glu-89, in addition to its direct interaction with the phosphate backbone of the template (cyan). Mutation of Trp to Tyr at position 153 reorients the side chain of Lys-154 (shown in red), resulting in the loss of these interactions. The Cα backbone is shown as thin lines, while the template, primer, and dNTP are shown in blue, gray, and orange, respectively.

positioned such that its mutation adversely affects RNase H activity without affecting the polymerase function of the enzyme (*57*), while the Phe → Leu substitution at position 77 confers resistance to nucleoside inhibitors (*58*). In crystal structure of the E−DNA binary complex, Phe-77 does not have any interaction with Trp-153, while Phe-77 is seen within interacting distance in the structure of the E−DNA−dNTP ternary complex. This implies that the hydrophobic core in the ternary complex is relatively more compact than in the binary complex. This compactness can be judged from the fact that in the ternary complex, the exposed surface areas of Tyr-115, Trp-153, and Ser-156 are 8, 5, and 6 Å^2, respectively, whereas upon complete exposure to the solvent, these residues acquire surface areas of 163, 181, and 98 Å^2, respectively. Therefore, it appears that substitution of the side chain at position 153 may affect the flexibility of this hydrophobic core by altering the exposed surface areas of its constituents. Although introduction of a Phe side chain at this position is tolerated well, abolition of a side chain (Trp → Ala) or introducing a polar side chain (Trp → Tyr) may disrupt the integrity of this hydrophobic core. A significant decrease in the apparent binding affinity for dNTP in the ternary complex observed with Trp → Tyr and Trp → Ala mutants could be a direct consequence of this alteration. These hydrophobic residues in or surrounding the catalytic pocket may play an important role in enhancing the ligand reactivity with the active site residues by facilitating the exclusion of water molecules. It has been suggested that exclusion of water molecules from the polymerase active site magnifies the free energy differences between the correct and incorrect base pairs, thereby contributing to higher polymerase fidelity (*59*). The perturbation of the hydrophobic core due to Trp → Try and Trp → Ala substitution at position 153 may be one of the factors responsible for the improved misinsertion and/or mispair extension abilities of these mutants.

Mutant modeling of the Trp → Tyr substitution at position 153 in the ternary complex crystal structure indicated a significant change in the conformation of the side chain of an adjacent residue, Lys-154 (Figure 8B). In the WT enzyme, Lys-154 ion pairs with Glu-89 and has a Coulombic interaction with the 5′-phosphate atom of the template nucleotide paired with the penultimate primer base. Glu-89 also interacts with the sugar−phosphate moiety of the same template nucleotide, in addition to its interaction with Gln-161, which in turn has van der Waals interactions with the primer base. The network of these interactions is perturbed by a single Trp → Tyr substitution at position 153, resulting in the reorientation of the side chain of Lys-154 (Figure 8B), thus disrupting its interaction with the template phosphate as well as the salt bridge interaction with Glu-89. This may well explain the reduction in both DNA binding and apparent dNTP binding affinities observed with both Trp → Ala and Trp → Tyr mutants.

Modeling of Ile-167 and Leu-187 mutant derivatives shows a slight positional change in the side chain of Met at position 164. In the WT enzyme, the side chain of Met-164 interacts with the backbone carbonyl of Met-184 (Figure 9A). Met-184, located at the β9−β10 turn in the active site pocket of HIV-1 RT, interacts with the sugar moiety of the dNTP substrate and has been suggested to play an important role in the fidelity of the enzyme (*31*, *32*, *34*, *60*, *61*). A natural Met → Val substitution at position 184 has been shown to confer the 3TC resistance phenotype to the enzyme (*54*, *58*, *62*). Comparison of the crystal structures of unliganded HIV-1 RT (apoenzyme) and DNA− or DNA−dNTP-bound HIV-1 RT indicates that upon binding to DNA, the β9−turn−β10 region of HIV-1 RT changes its position significantly (approximately 2.0 Å; Figure 9B), thus resembling a "springboard" conformation (*19*). In this conformation, Met-164 interacts with the backbone C═O group of Met-184 and thus appears to stabilize this conformation which, in turn, may be required for the stabilization of the ternary complex. Substitutions at position 167 or 187 may alter the position of Met-164, resulting in the loss of the interaction between the side chain of Met-164 and the backbone of Met-184. The loss of this interaction may destabilize the loop between β9 and β10 in its "pushed" position and thus may alter the binding affinity for substrates in the case of the mutant enzymes. Therefore, the influence of the mutations at Ile-

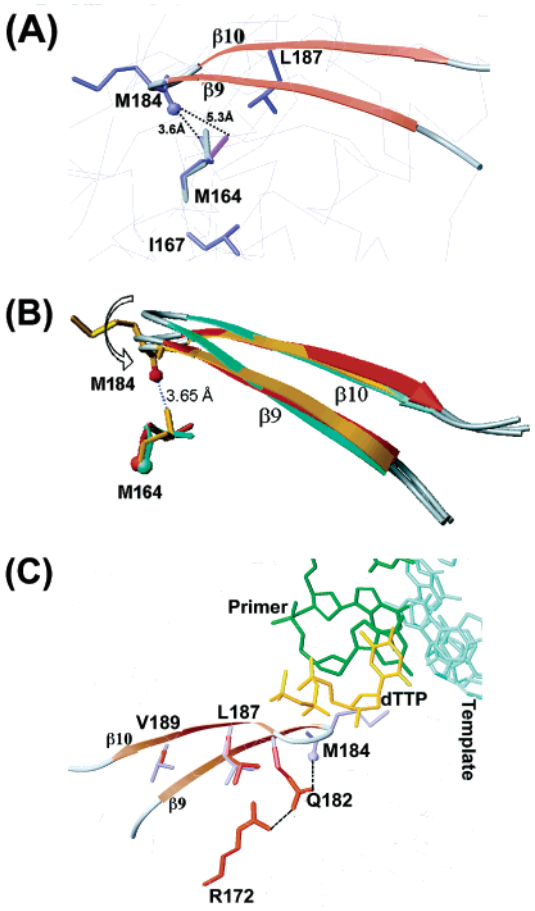

FIGURE 9: Effect of mutations at positions 167, 187, and 189 on the side chain orientation of the neighboring residues. Mutant modeling was performed using Look version 3.5 (Molecular Application Group) and the apo, binary, and ternary complex crystal structures corresponding to PDB entries 1hmv, 2hmi, and 1rtd, respectively. (A) Changes in the side chain of Met-164 upon substitution of Ile-167 with Ala-167 (blue) or Leu-187 with Ala-187 (magenta) are as shown. The side chain of Met-164 is positioned between the side chains of Ile-167 and Leu-187. The H-bond between the backbone of Met-184 and the side chain of Met-164 is shown with dotted lines. The backbone carbonyl atom of Met-184 is shown as a ball. Mutation of Ile-167 or Leu-187 appears to change the conformation of the side chain of Met-164, resulting in disturbance of the H-bonding interaction and thus reducing the stability of the loop in the specific springboard conformation described in panel B. (B) In the wild-type enzyme, the loop between β9 and β10 assumes a springboard conformation upon binding to DNA or DNA and dNTP (*12*). This change in the conformation appears to be stabilized by the hydrogen bond between the backbone carbonyl atom of Met-184 and the side chain of Met-164. The position of the loop between the two β-strands in the apoenzyme (cyan) is pushed down upon DNA binding (orange-red). The change in the position of the Cα atom of M184 is $\sim$1.9 Å which further changes upon dNTP binding (gold). (C) Mutant modeling at position 189 (V189A) appears to alter the side chain of Leu-187, which interacts with the Cβ atom of Q182 in the crystal structure of the wild-type enzyme. The side chain of Gln-182, similar to Met-164, forms a hydrogen bond with the backbone carbonyl atom of Met-184 in the ternary complex, suggesting the indirect involvement of Val-189 in positioning the primer as well as dNTP via these residues. In addition, Gln-182 also has the potential to form hydrogen bond with Arg-172. The template, primer, and dTTP are shown in cyan, green, and orange, respectively. Except for residues Gln-182 and Arg-172, the other side chains in the wild-type enzyme are shown in blue. The change in the side chain of Leu-187 with the V189A mutation is shown in red.

167 and Leu-187 on DNA binding, stable ternary complex formation, and apparent dNTP binding affinity may be a consequence of an indirect effect via subtle change in the interaction between the two methionine residues at positions 164 and 184.

Modeling of the mutant derivatives of Val-189 exhibited no significant change in the orientation of other residues in its vicinity, with the sole exception of Leu-187. In the WT enzyme, the C$_\beta$ atom of Leu-187 interacts hydrophobically with the aliphatic carbon chain of Gln-182 which, in turn, has H-bond interaction with the carbonyl backbone of Met-184, located on the β9$-\beta$10 loop (Figure 9C). Thus, any perturbation in this interaction would lead to a more relaxed position of the β9$-\beta$10 loop, thereby conferring greater flexibility to the DNA and dNTP binding pockets. A more flexible pocket may be less discriminatory with respect to nucleotide selection (*28*). Our results with the mutant derivatives of Val-189 support this contention.

In summary, our results indicate that these hydrophobic residues on motifs B and C of HIV-1 RT are important for maintaining the geometry of the DNA and dNTP binding pocket. The increased sensitivity of their nonconserved mutants to nevirapine explains the absence of naturally occurring mutations at these positions in response to drug therapy.

REFERENCES

1. Parniak, M. A., and Sluis-Cremer, N. (2000) *Adv. Pharmacol. 49*, 67−109.
2. Arts, E. J., and Le Grice, S. F. J. (1998) *Prog. Nucleic Acids Res. Mol. Biol. 58*, 339−393.
3. Telesnitsky, A., and Goff, S. P. (1997) in *Retroviruses* (Coffin, J., Hughes, S. H., and Varmus, H., Eds.) pp 121−160, Cold Spring Harbor Laboratory Press, Plainview, NY.
4. di Marzo Veronese, F., Copeland, T. D., DeVico, A. L., Rahman, R., Oroszlan, S., Gallo, R. C., and Sarngadharan, M. G. (1986) *Science 231*, 1289−1291.
5. Varmus, H. E. (1985) *Nature 314*, 583−584.
6. Ferris, A. L., Hizi, A., Showalter, S. D., Pichuantes, S., Babe, L. Craik, C. S., and Hughes, S. H. (1990) *Virology 175*, 456−464.
7. Kohlstaedt, L. A., Wang, J., Friedman, J. M., Rice, P. A., and Steitz, T. A. (1992) *Science 256*, 1783−1790.
8. Restle, T., Muller, B., and Goody, R. S. (1990) *J. Biol. Chem. 265*, 8986−8988.
9. Beard, W. A., and Wilson, S. H. (1993) *Biochemistry 32*, 9745−9753.
10. Pandey, P. K., Kaushik, N., Talele, T. T., Yadav, P. N. S., and Pandey, V. N. (2001) *Biochemistry 40*, 9505−9512.
11. Rodgers, D. W., Gamblin, S. J., Harris, B. A., Ray, S., Culp, J. S., Hellmig, B., Woolf, D. J., Debouck, C., and Harrison, S. C. (1995) *Proc. Natl. Acad. Sci. U.S.A. 92*, 1222−1226.
12. Hsiou, Y., Ding, J., Das, K., Clark, A. D., Hughes, S. H., and Arnold, E. (1996) *Structure 4*, 853−860.
13. Smerdon, S. J., Jager, J., Wang, J., Kohlstaedt, L. A., Chirino, A. J., Friedman, J. M., Rice, P. A., and Steitz, T. A. (1994) *Proc. Natl. Acad. Sci. U.S.A. 91*, 3911−3915.
14. Ding, J., Das, K., Moereels, H., Koymans, L., Andries, K., Janssen, P. A., Hughes, S. H., and Arnold, E. (1995) *Nat. Struct. Biol. 2*, 407−415.
15. Ding, J., Das, K., Tantillo, C., Zhang, W., Clark, A. D., Jr., Jessen, S., Lu, X., Hsiou, Y., Jacobo-Molina, A., Andries, K., Pauwels, R., Moereels, H., Koymans, L., Janssen, P. A. J., Smith, R. H., Jr., Koepke, M. K., Michejda, C. J., Hughes, S. H., and Arnold, E. (1995) *Structure 3*, 365−379.
16. Ren, J., Esnouf, R., Garman, E., Somers, D., Ross, C., Kirby, I., Keeling, J., Darby, G., Jones, Y., Stuart, D., and Stammers, D. (1995) *Nat. Struct. Biol. 2*, 293−302.
17. Sarafianos, S. G., Das, K., Tantillo, C., Clark, A. D., Jr., Ding, J., Whitcomb, J. M., Boyer, P. L., Hughes, S. H., and Arnold, E. (2001) *EMBO J. 20*, 1449−1461.

18. Ding, J., Hughes, S. H., and Arnold, E. (1997) *Biopolymers 44*, 125−138.
19. Ding, J., Das, K., Hsiou, Y., Sarafianos, S. G., Clark, A. D., Jr., Jacobo-Molina, A., Tantillo, C., Hughes, S. H., and Arnold, E. (1998) *J. Mol. Biol. 284*, 1095−1111.
20. Huang, H., Chopra, R., Verdine, G. L., and Harrison, S. C. (1998) *Science 282*, 1669−1675.
21. Carroll, S. S., Cowart, M., and Benkovic, S. J. (1991) *Biochemistry 30*, 804−813.
22. Drosopoulos, W. C., and Prasad, V. R. (1996) *J. Virol. 70*, 4834−4838.
23. Drosopoulos, W. C., and Prasad, V. R. (1998) *J. Virol. 72*, 4224−4230.
24. Ding, J., Das, K., Yadav, P. N. S., Hsiou, Y., Zhang, Y., Zhang, W., Hughes, S. H., and Arnold, E. (1997) A review of HIV-1 RT structural studies and implications for drug design, in *Structure Based Drug Design* (Veerapandian, P., Ed.) pp 41−82, Marcel Dekker, New York.
25. Kaushik, N., Harris, D., Rege, N., Modak, M. J., Yadav, P. N. S., and Pandey, V. N. (1997) *Biochemistry 36*, 14430−14438.
26. Kaushik, N., Talele, T. T., Pandey, P. K., Harris, D., Yadav, P. N. S., and Pandey, V. N. (2000) *Biochemistry 39*, 2912−2920.
27. Kim, B., Ayran, J.-C., Sagar, S. G., Adman, E. T., Fuller, S. M., Tran, N. H., and Horrigan, J. (1999) *J. Biol. Chem. 274*, 27666−27673.
28. Harris, D., Kaushik, N., Pandey, P. K., Yadav, P. N. S., and Pandey, V. N. (1998) *J. Biol. Chem. 273*, 33624−33634.
29. Larder, B. A., and Kemp, S. D. (1989) *Science 246*, 1155−1158.
30. Kew, Y., Salomon, H., Olsen, L. R., Wainberg, M. A., and Prasad, V. R. (1996) *Antimicrob. Agents Chemother. 40*, 1711−1714.
31. Pandey, V. N., Kaushik, N., Rege, N., Sarafianos, S. G., Yadav, P. N. S., and Modak, M. J. (1996) *Biochemistry 35*, 2168−2179.
32. Wainberg, M. A., Drosopoulos, W. C., Salomon, H., Hsu, M., Borkow, G., Parniak, M., Gu, Z., Manme, J., Islam, S., Castriota, G., and Prasad, V. R. (1996) *Science 271*, 1282−1285.
33. Rezende, L. F., Curr, K., Ueno, T., Mitsuya, H., and Prasad, V. R. (1998) *J. Virol. 72*, 2890−2895.
34. Rezende, L. F., Drosopoulos, W. C., and Prasad, V. R. (1998) *Nucleic Acids Res. 26*, 3066−3072.
35. Tisdale, M., Kemp, S. D., Parry, N. R., and Larder, B. A. (1993) *Proc. Natl. Acad. Sci. U.S.A. 90*, 5653−5656.
36. Gu, Z., Gao, Q., Fang, H., Salomon, H., Parniak, M. A., Goldberg, E., Cameron, J., and Wainberg, M. A. (1994) *Antimicrob. Agents Chemother. 38*, 275−281.
37. Tantillo, C., Ding, J., Jacobo-Molina, A., Nanni, R. G., Boyer, P. L., Hughes, S. H., Pauwels, R., Andries, K., Janssen, P. A., and Arnold, E. (1994) *J. Mol. Biol. 243*, 369−387.
38. Balzarini, J. (1999) *Biochem. Pharmacol. 58*, 1−27.
39. Jonckheere, H., Anne, J., and De Clercq, E. (2000) *Med. Res. Rev. 20*, 129−154.
40. Kleim, J.-P., Rosner, M., Winkler, I., Paessens, A., Kirsch, R., Hsiou, Y., Arnold, E., and Riess, G. (1996) *Proc. Natl. Acad. Sci. U.S.A. 93*, 34−38.
41. Arts, E. J., Li, X., Gu, Z., Kleiman, L., Parniak, M. A., and Wainberg, M. A. (1994) *J. Biol. Chem. 269*, 14672−14680.
42. Chattopadhyay, D., Evans, D. B., Diebel, M. R., Jr., Vosters, A. F., Eckenrode, F. M., Einspahr, H. M., Hui, J. O., Tomasselli, A. G., Zurcher-Neely, H. A., Heinrikson, R. L., and Sharma, S. K. (1992) *J. Biol. Chem. 267*, 14227−14232.
43. Lee, R., Kaushik, N., Modak, M. J., Vinayak, R., and Pandey, V. N. (1998) *Biochemistry 37*, 900−910.
44. Astatke, M., Grindley, N. D. F., and Joyce, C. M. (1995) *J. Biol. Chem. 270*, 1945−1954.
45. Tong, W. W., Lu, C., Sharma, S. K., Matsuura, S., So, A. G., and Scott, W. A. (1997) *Biochemistry 36*, 5749−5757.
46. Sanger, F., Nicklen, S., and Coulson, A. R. (1977) *Proc. Natl. Acad. Sci. U.S.A. 74*, 5463−5467.
47. Kati, W. M., Johnson, K. A., Jerva, L. F., and Anderson, K. S. (1992) *J. Biol. Chem. 267*, 25988−25997.
48. Weiss, K. K., Bambara, R. A., and Kim, B. (2002) *J. Biol. Chem. 277*, 22662−22669.
49. Mellors, J. W., Bazmi, H. Z., Schinazi, R. F., Roy, B. M., Hsiou, Y., Arnold, E., Weir, J., and Mayers, D. L. (1995) *Antimicrob. Agents Chemother. 39*, 1087−1092.
50. Gutierrez-Rivas, M., Ibanez, A., Martinez, M. A., Domingo, E., and Menendez-Arias, L. (1999) *J. Mol. Biol. 290*, 615−625.
51. Tramontano, E., Piras, G., Mellors, J. W., Putzolu, M., Bazmi, H., and La Colla, P. (1998) *Biochem. Pharmacol. 56*, 1583−1589.
52. Wrobel, J. A., Chao, S. F., Conrad, M. J., Merker, J. D., Swanstrom, R., Pielak, G. J., and Hutchison, C. A., III (1998) *Proc. Natl. Acad. Sci. U.S.A. 95*, 638−645.
53. Chao, S. F., Chan, V. L., Juranka, P., Kaplan, A. H., Swanstrom, R., and Hutchison, C. A., III (1995) *Nucleic Acids Res. 23*, 803−810.
54. Ueno, T., and Mitsuya, H. (1997) *Biochemistry 36*, 1092−1099.
55. Boyer, P. L., Ferris, A. L., Clark, P., Whitmer, J., Frank, P., Tantillo, C., Arnold, E., and Hughes, S. H. (1994) *J. Mol. Biol. 243*, 472−483.
56. Weiss, K. K., Isaacs, S. J., Tran, N. H., Adman, E. T., and Kim, B. (2000) *Biochemistry 39*, 10684−10694.
57. Boyer, P.-L., Ferris, A. L., and Hughes, S. H. (1992) *J. Virol. 66*, 1031−1039.
58. Ueno, T., Shirasaka, T., and Mitsuya, H. (1995) *J. Biol. Chem. 270*, 23605−23610.
59. Petruska, J., Sowers, L. C., and Goodman, M. F. (1986) *Proc. Natl. Acad. Sci. U.S.A. 83*, 1559−1562.
60. Bakhanashvili, M., Avidin, O., and Hizi, A. (1996) *FEBS Lett. 391*, 257−262.
61. Feng, J. Y., and Anderson, K. S. (1999) *Biochemistry 38*, 9440−9448.
62. Larder, B. A., Kemp, S. D., and Harrigan, P. R. (1995) *Science 269*, 696−699.

BI026311Z